Computational aspects of many-body potentials

Steven J. Plimpton and Aidan P. Thompson

We discuss the relative complexity and computational cost of several popular many-body empirical potentials, developed by the materials science community over the past 30 years. The inclusion of more detailed many-body effects has come at a computational cost, but the cost still scales linearly with the number of atoms modeled. This is enabling very large molecular dynamics simulations with unprecedented atomic-scale fidelity to physical and chemical phenomena. The cost and scalability of the potentials, run in serial and parallel, are benchmarked in the LAMMPS molecular dynamics code. Several recent large calculations performed with these potentials are highlighted to illustrate what is now possible on current supercomputers. We conclude with a brief mention of high-performance computing architecture trends and the research issues they raise for continued potential development and use.

Introduction

Since the mid-1990s, Pixar Animation Studios has created and released 12 full-length animated movies.[1] Aficionados of computer-generated imagery (CGI) are aware that several of their movies have pushed the boundaries of what can be realistically animated. Examples include vegetation ("A Bug's Life"), fabric ("Toy Story 2"), hair ("Monsters, Inc."), water ("Finding Nemo"), surfaces with layers of paint and dirt ("Cars"), food ("Ratatouille"), and rust and decay ("WALL-E").[2]

Interestingly, as processor speeds and the number of processors used by Pixar have increased, the time needed to render the individual frames of its movies has not decreased. This is because the animators exploit increased computational power to render more complex physics and more complex scenes in each image. One of their employees referred to this as the "Law of Constancy of Pain."[3] With continued enhancements to their algorithms and software, Pixar is moving toward the goal of enabling fast, realistic rendering of any physical phenomenon with a minimum of effort by the animator. Their algorithm developers are adept at knowing what low-level expensive details can be discarded while still producing images that "look right." An important part of this process is comparing the animated images to real life, whether it be live video of swimming fish or human actors and their facial expressions.

As fans of Pixar films know, the company's success (nearly two dozen Academy Awards and an average gross of $600 million per film) is not simply due to their animation prowess, but to their ability to use animation as a tool to tell an entertaining story that appeals to children and adults alike.

Some parallels to computational materials science and, in particular, to the growing use of many-body potentials in atomistic modeling, are evident. Over the 30 years covered in this issue of *MRS Bulletin*, and leveraging the same increases in computational power available to Pixar, the scope and fidelity of atomistic materials modeling has grown by leaps and bounds. This is true both of the length and timescales accessible to simulation, as well as the complexity of the underlying physics encoded in a growing suite of empirical potentials.

A key motivation for developers of new potentials has been to enable more accurate modeling of specific classes of materials such as metals, ceramics, oxides, or carbon nanotubes, often by including many-body effects. Part of the art and acumen needed in the development process is to know what physics and chemistry to include to capture the desired physical effects but also what can be excluded to enhance computational efficiency. Simulations using empirical potentials have to do more than just "look right;" quantitative accuracy is required for comparisons with experiments or to more expensive and smaller-scale quantum calculations.

For simulators, the analog of the "Law of Constancy of Pain" is that while computing power has grown over time, the amount of wall-clock time available to an individual researcher on large computing platforms has not. Nor has our patience to wait for results. Most researchers do not use today's computers to

Steven J. Plimpton, Sandia National Laboratories, Albuquerque, NM; email sjplimp@sandia.gov
Aidan P. Thompson, Scalable Algorithms Department, Sandia National Laboratories, Albuquerque, NM; athomps@sandia.gov
DOI: 10.1557/mrs.2012.96

© 2012 Materials Research Society

simply run 10-year-old models faster than they did 10 years ago. Rather, they want to exploit increased computational resources by running larger systems for longer time scales, using more sophisticated potentials, while still waiting at most a few hours or days for the results.

At its best, atomistic modeling is a tool for telling a good science story (e.g., understanding for the first time the mechanisms underlying some physical phenomenon) or enabling models of processes that in turn allow more efficient or controllable manufacture of materials of interest. Sadly, this is the point where the Pixar analogy breaks down. To our knowledge, no developer of a many-body potential has yet been nominated for an Academy Award or received a grant for $600 million.*

In this article, we illustrate aspects of computational advances in atomistic modeling enabled by many-body potentials. In the next section, we discuss computational attributes of several popular potentials, developed over the last 30 years, and benchmark their relative cost and scalability for use in large simulations. In the subsequent section, we show results from several large-scale calculations to give the reader a sense of the current state-of-the-art for atomistic modeling with many-body potentials. We conclude with comments about how future hardware and software trends may influence continued research efforts in this area.

Computational performance

Before many-body potentials, there were pair or two-body potentials. Classic examples are the Lennard-Jones 6–12 potential (LJ)[4] (for van der Waals interactions) and Coulombic interactions between charged particles. It is worth noting these two potentials are still commonly used for modeling non-bonded interactions in all-atom biological and polymeric simulations (e.g., for solvated proteins). In force fields, such as CHARMm[5] and AMBER,[6] for these systems, the non-bond terms are augmented by a list of permanent bonds within each molecule's topology, connected by harmonic springs. Additional terms represent covalent bond bending and torsion energies.

In contrast, many-body potentials, as the name implies, explicitly include many-body effects. The energy expression for the potential is typically written as a sum over interactions that involve not just two, but clusters of three or more nearby atoms. Unlike the permanent bonds in biological models, the atoms participating in each interaction depend on their current configuration, so that covalent bonds can effectively break and form again as atoms move.

Table I lists eight such many-body potentials, the year they were first published, materials they are commonly used to model, and a typical time step size when used in a molecular dynamics simulation. The SPC/E water potential, used in biomolecular models, is included for comparison; it is computed via pairwise LJ and Coulombic interactions with additional constraints to rigidify each molecule. We next describe a few salient features of these many-body potentials that impact their computational cost. The timing information in the table is discussed later in the text.

The embedded-atom method (EAM) potential[7,8] combines a pairwise interaction with a second term representing the energy of embedding each atom in the electron density produced by its neighbors. This term elegantly captures the compressibility of the electron gas formed by valence electrons in metals, without resorting to a special volume-dependent energy term. Computing this embedding energy and its derivative (force) requires two computational loops over neighbors: one to sum electron densities so the embedding function can be evaluated for each atom, and a second to calculate the force on each atom due to its contribution to its neighbors' embedding energies. This is the source of the effective many-body nature of the potential and a common computational motif in all the potentials discussed here (see the sidebar).

Tersoff test

Two criteria that can be used to help identify particularly effective inter-atomic potential energy functions have been attributed to Jerry Tersoff, one of the early developers of bond order potentials. These criteria are (1) "Has the person who constructed the potential subsequently refined the potential based on initial simulations?" and (2) "Has the potential been used by other researchers for simulations of phenomena for which the potential was not designed?"(B.J. Garrison, D. Srivastava, *Ann. Rev. Phys. Chem.* **46**, 373 [1995]). Meeting these two criteria suggests that a potential has been thoroughly vetted, and that the developer has fixed any problems that were identified. Almost all of the potential functions discussed in this issue pass the Tersoff test.

The modified EAM (MEAM) potential[9] has a similar mathematical structure to EAM, except that the electron density is given by a more complicated expression involving sums over three-body contributions that depend on the angle θ_{ijk} subtended by atoms j and k at a central atom i.

The Tersoff potential[10] uses a short-range pair potential to represent covalent bonding. The key innovation is the concept of bond order, which plays a central role in many-body potentials such as BOP (bond-order potential) and REBO (reactive empirical bond order) and ReaxFF (reactive force field) potentials. In the Tersoff potential, the energy of a bond is modulated by the angular location of neighbor atoms relative to the bond axis.

* The comparison can also be stretched too far in the other direction. The analog for computer design of new materials would be to use CGI to create an improved version of George Clooney or Meryl Streep, something not even Pixar is likely planning.

Table I. Many-body potentials.

Potential	Year	Materials	Benchmark	Time Step (fs)	CPU (secs/atom/step)	Ratio (to LJ)	50% Eff (atoms/proc)
EAM	1983[7]	fcc metals	Cu	5.0	$3.52\ 10^{-6}/3.44\ 10^{-6}$	2.3x	500
MEAM	1987[9]	metals	Ni	5.0	$3.04\ 10^{-5}/3.08\ 10^{-5}$	20x	125
Tersoff	1988[10]	covalent solids	Si	1.0	$7.13\ 10^{-6}/7.32\ 10^{-6}$	4.6x	125
REBO	1990[11]	CNTs	polyethylene	0.5	$1.34\ 10^{-5}/1.35\ 10^{-5}$	8.7x	125
BOP	1999[13]	covalent solids	CdTe	1.0	$5.05\ 10^{-5}/4.66\ 10^{-5}$	33x	50
AIREBO	2000[12]	multiwall CNTs	polyethylene	0.5	$8.28\ 10^{-5}/8.42\ 10^{-5}$	54x	100
ReaxFF	2001[14]	universal	PETN crystal	0.1	$3.94\ 10^{-4}/4.43\ 10^{-4}$	256x	300
COMB	2007[15]	oxides, interfaces	SiO_2	0.2	$9.00\ 10^{-4}/8.83\ 10^{-4}$	585x	25
SPC/E	1987[42]	water	liquid H_2O	2.0	$2.01\ 10^{-5}/1.93\ 10^{-5}$	13x	500

Many-body potentials (except SPC/E) discussed in this article, with their publication date, typical materials they model, and time step size for molecular dynamics simulation. The two CPU times are for small (32 K atom) and large (1 M atom) simulations. The ratio is the small-problem CPU time relative to a simple Lennard-Jones potential. The 50% efficiency metric is taken from Figure 1.
EAM, embedded-atom method; MEAM, modified embedded-atom method; REBO, reactive empirical bond order; BOP, bond–order potential; AIREBO, adaptive intermolecular REBO; ReaxFF, reactive force field; COMB, charge optimized many-body; CNT, carbon nanotube.

The REBO potential[11] extends the bond-order approach to differentiate between σ and π bonds, which increases the stability and torsional stiffness of double and triple carbon-carbon bonds. The adaptive intermolecular REBO (AIREBO) potential[12] extends the REBO potential by adding dispersion interactions between nearby atoms leading to effective six-body interactions. The BOP[13] uses the tight-binding theory of bond formation to describe the energetics of covalently bonded materials.

The ReaxFF potential[14] is a variable-charge bond order potential. In addition to handling conventional covalent bonding contributions, such as bond formation, stretching, bending, and torsion, it also explicitly represents a range of additional chemical bonding features, such as hydrogen bonding and bond conjugation. Charge equilibration is handled by the iterative solution of a linear system of equations representing the electronegativity equalization conditions. The need to compute long-range electrostatic interactions is eliminated by using a smoothly truncated Coulombic potential.

The charge-optimized many-body potential (COMB)[15] is also a variable charge bond-order potential, developed to treat interfaces, oxides, and other compounds. The charges on atoms are adjusted at each time step according to the electronegativity equalization method,[16] which minimizes the total electrostatic energy of the system. Computation of long-range electrostatics is avoided by using the short-range Wolf summation method.[17]

These are computational issues associated with these many-body potentials, which increase their complexity and cost:

- As the level of many-body dependencies increases, multiple and/or nested computational loops are needed to identify neighbors, neighbors of neighbors, etc. This likewise implies longer cutoff distances as atoms are influenced by atoms further away.
- As discussed for the EAM potential, there are intermediate stages to the computations where many-body terms are summed over interactions. In parallel, this typically requires extra communication to acquire the terms from atoms owned by different processors.
- Identifying nearby groups of atoms that interact often requires that each atom store a "full" list of all its neighbors, rather than the typical "half" lists that suffice for enumerating pairwise interactions, due to pairwise forces being equal and opposite.
- For potentials that include variable charge (e.g., ReaxFF and COMB), charge equilibration is effectively a long-range interaction that incurs additional cost. However, computing true long-range Coulombics (e.g., via an Ewald summation[18]) is avoided by the use of approximate methods that truncate interactions within a cutoff distance.

The potentials in Table I have all been implemented in our parallel molecular dynamics (MD) package LAMMPS,[19,20] which allows us to compare their computational cost.[†] One feature of LAMMPS that makes it attractive for use in materials modeling is that it was designed to allow users to easily add functionality, such as a new potential, through well-defined interfaces. Evidence of this is that several of the potentials in Table I were implemented by individuals, including students, with only limited interaction with the LAMMPS developers.

The author of a potential writes code that computes per-atom forces and energies, as well as sets up or reads user-defined parameters (e.g., from a file). The LAMMPS infrastructure provides neighbor lists of various kinds, enables the potential to be used in hybrid simulations where two or more potentials are used to compute interactions between different groups of

[†] The benchmarks timings presented are for second-generation REBO[21] and second-generation COMB[22] potentials, which are later versions than the dates listed in Table I. Recent enhancements to the COMB implementation in LAMMPS show speed-ups of about 2x relative to what is presented here, but our Cray XT5 machine was not available to re-run the benchmarks.

atoms (e.g., water or polymer chains on a metal surface), performs time integration, and computes additional analyses or diagnostics as requested by the user. Diagnostics can include per-atom virials and total energy and pressure, which can be derived from the per-atom energies and forces, eliminating the need for the potential itself to tally these quantities.[23]

We benchmarked the relative computational cost of the LAMMPS implementation of the potentials in Table I on a Cray XT5 at Sandia National Laboratory. In each case, we ran a prototypical problem for that potential for 100 time steps, which is long enough to amortize the cost of occasional tasks such as neighbor-list building. More details on the benchmark problems are given in Reference 19, which include timing data for other pairwise and many-body potentials not discussed here.

The results are shown in **Figure 1**. For each potential, three benchmark tests were performed. The "small" (red) and "large" (green) curves are for 32,000 (32 K) and 1,000,000 (1 M) atom systems, respectively (small variations in size for different crystal structures), run on varying numbers of processors (so-called strong-scaling results). The "scaled" (blue) curves are for systems whose size (32,000 atoms per processor) was increased in proportion to the number of processors (weak-scaling results). Thus their 1024-processor timings are for 32 M atom systems.

The plots show parallel efficiencies, where for each potential the one-processor timing is assumed to be 100% efficient (dotted lines). For the strong-scaling (red/green) curves, parallel efficiency is defined as the one-processor CPU time T_1 divided by the P-processor time T_P, multiplied by $(100/P)$. Thus a 1024-processor efficiency of 50% means the 32 K- or 1 M-atom problem ran 512 times faster than it did on one processor. For the weak-scaling (blue) curves, parallel efficiency is simply $100\ T_1/T_P$, so that a 50% value means the 32 M-atom problem ran two times slower on 1024 processors than the 32 K-atom problem did on one processor.

Note that single-processor CPU times vary greatly between the potentials, as listed in Table I, normalized on a per-atom, per-time step basis. Also note that the typical time step size is different for different potentials. These timings are for full

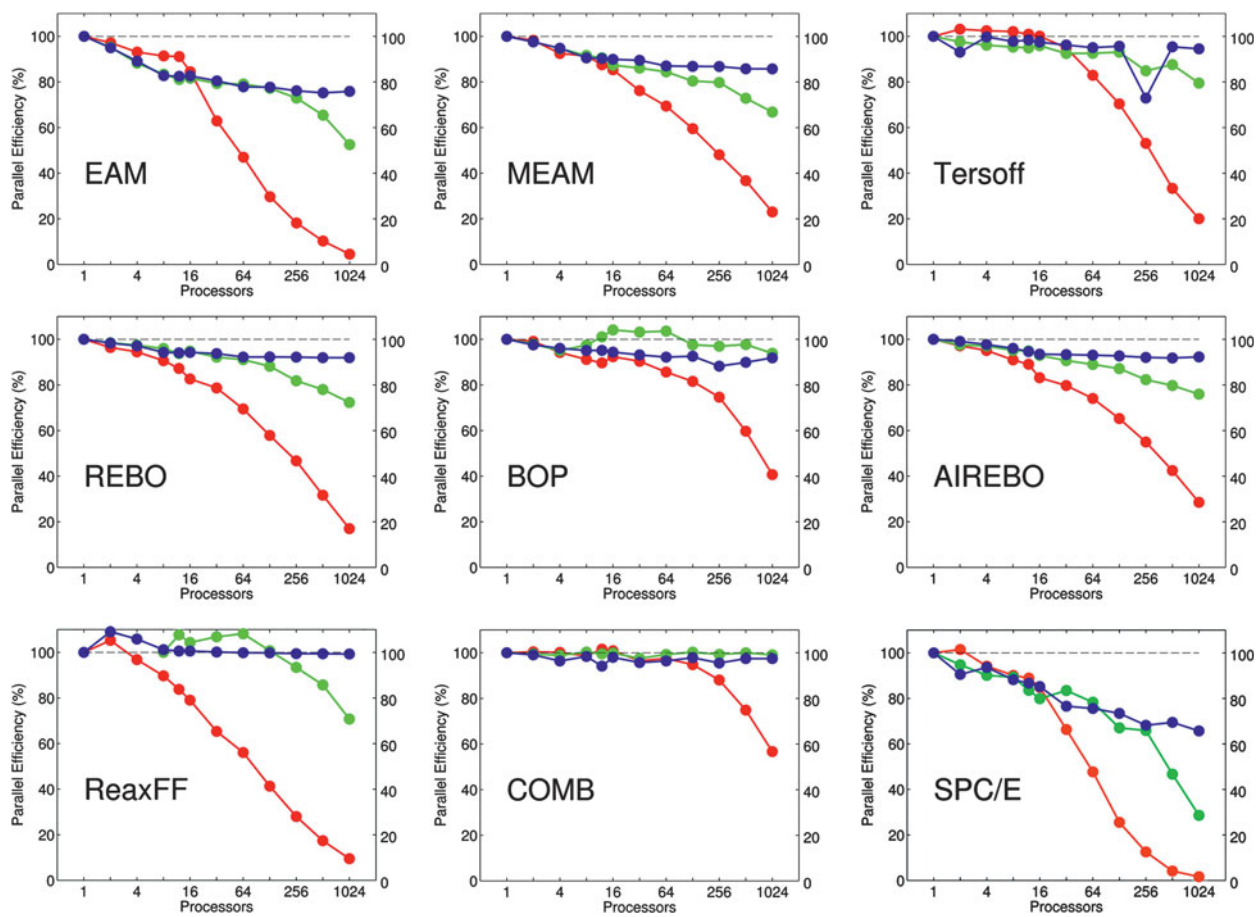

Figure 1. Performance of eight many-body potentials and an SPC/E water potential on varying numbers of cores of a Cray XT5 machine, as implemented in LAMMPS.[19] The red curves are for 32 K-atom systems; the green curves are for 1 M-atom systems; and the blue curves are for scaled systems with 32 K atoms per processor. Definitions of fixed-size and scaled-size parallel efficiency and the dotted line are discussed in the text. Single-core CPU times per-atom per-time step are listed in Table I. EAM, embedded-atom method; MEAM, modified embedded-atom method; REBO, reactive empirical bond-order; BOP, bond order potential; AIREBO, adaptive intermolecular REBO; ReaxFF, reactive force field; COMB, charge optimized many-body.

simulations, which include the cost of neighbor-list building and time integration. However, the vast majority of time, even for the cheapest potentials, is spent in computing the many-body interactions.

Several trends are evident from the plots in Figure 1:

- The weak-scaling (blue) curves for all the many-body potentials show excellent scalability as the problem size and processor counts increase. This is because all of them, even the expensive ones, are essentially short-range in nature. (The nominally long-range charge-equilibration calculations for ReaxFF and COMB do not affect this, at least for these benchmark problems.) This means their computational complexity scales linearly with N/P for the number of atoms N and processors P, so long as there are sufficient atoms per processor. This is also reflected in the single-processor timings listed in Table I, which are nearly identical for the small 32 K- and large 1 M-atom problems, when normalized on a per-atom basis. The one exception is the blue curve for SPC/E. The degradation in efficiency is due to the long-range Coulombic calculation performed via the particle-particle, particle-mesh (PPPM) method[24,25] in LAMMPS, or the related particle-mesh Ewald (PME) method[26] in other MD codes. These are FFT-based methods with an $O(N\log N)$ complexity in the number of atoms, so their cost grows as the system size increases.
- The strong-scaling curves show reasonable scalability until the efficiency rolls off as the number of atoms per processor becomes too small. This happens more quickly for the 32 K-atom problem (red) than for the 1 M-atom problem (green) and for cheaper potentials than for more expensive ones. Again, the SPC/E potential has the worst strong-scaling behavior, due to the high communication costs of the parallel 3D FFTs needed for long-range Coulombic calculations.
- Many of the curves show different efficiency behavior for fewer versus more than 12 processors. This is typical of the performance of many codes on multi-core nodes and reflects the architecture of the compute nodes in our Cray XT5, which contain dual hex-core processors (12 cores/node). Within a single node, running in parallel on more cores incurs memory-bandwidth bottlenecks that degrade single-node performance. In weak-scaling mode (blue), adding nodes does not degrade performance further, since the additional time spent on inter-node communication remains small relative to the computation. However, for the strong-scaling results (red), adding more nodes reduces the number of atoms per node, which can degrade efficiency more rapidly if the inter-node communication is more costly than the reduced on-node computation.

The overall message of these benchmarking data is that many-body potentials perform or scale in molecular dynamics calculations with a cost that increases linearly with the number of atoms, which means very large calculations can be performed. The data from the table and plots can be used to estimate the time to run any size system on a given number of processors, so long as there are a few hundred atoms or more per processor (less for more expensive potentials). The last column in Table I shows an estimate of the threshold for each potential, from the 32 K-atom timings, to maintain a parallel efficiency of 50% or greater.

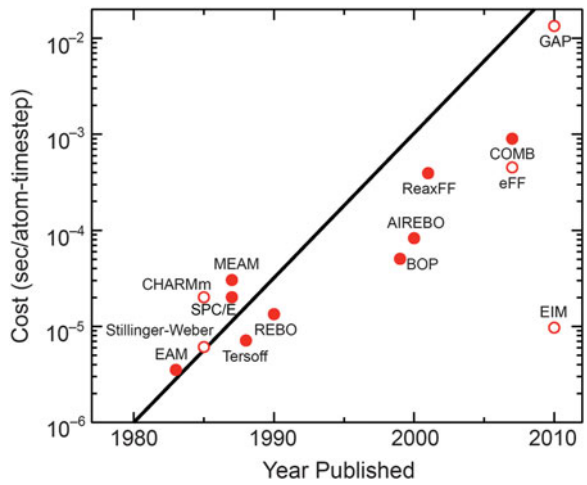

Figure 2. Single CPU cost in seconds per-atom per-time step versus year for the potentials of Table I (closed symbols) and others (open symbols). The line represents a doubling in computational cost every two years, akin to Moore's Law for hardware complexity.[19] EAM, embedded-atom method; MEAM, modified embedded-atom method; REBO, reactive empirical bond order; BOP, bond-order potential; AIREBO, adaptive intermolecular REBO; ReaxFF, reactive force field; COMB, charge optimized many-body; GAP, Gaussian approximation potential.

Another way to illustrate the growing computational complexity of many-body potentials over time is with the plot in **Figure 2**, similar to the familiar Moore's law for the exponential growth of transistor counts in semiconductor chips. The years and timings are taken from Table I for the small-system runs on a single Cray XT5 processor. The closed symbols are for potentials discussed here; the open symbols are for other (mostly many-body) potentials available in LAMMPS.[19] One exception is the new Gaussian-approximation potential or GAP, which is not yet available in the public distribution of LAMMPS.

It is important to note these are timings for running all of the potentials on today's hardware. If they were timings from the year they were developed, the slope in the data points would be closer to flat. Table I also gives a ratio of the CPU cost for the many-body potentials relative to the Lennard-Jones 6–12 pairwise potential,[4] which runs at 1.54×10^{-6} s/atom/time step in LAMMPS (for a liquid state point).[‡]

The GAP potential[27] shown at the upper right of Figure 2 was developed in 2010 with the goal of providing near quantum-level accuracy in an empirical potential for systems it is appropriately fit to via comparison to a large database of quantum-calculated energies and forces, as illustrated in

[‡] Since the LJ potential was published in 1924, we did not include it in the plot; it is an outlier in our otherwise compelling Moore's law analysis!

Figure 3 of Reference 27. It continues the trend of Figure 2, since our preliminary investigations indicate that evaluating its large set of spherical-harmonic basis functions is an order-of-magnitude more expensive than any of the many-body potentials in Table I.

The cost of empirical potentials can also be compared to quantum density functional theory (DFT) calculations. A collaborator, Thomas Mattsson at Sandia National Laboratory, gave CPU timings for several large systems he has recently modeled[28,29] via quantum dynamics calculations with the VASP program,[30] using a 1 fsec time step similar to atomistic molecular dynamics. For systems with 192 and 432 atoms (1024 and 3456 electrons), the CPU times/atom/step were 252 and 1344 seconds, respectively. These single processor times were inferred from parallel runs on 384 processors, assuming 100% parallel efficiency, since they required too much memory to run on a single processor. The runs were made on a Nehalem-based Linux cluster, with single-processor performance similar to the Cray XT5 used for the atomistic simulations.

On a per-atom per-time step basis, these timings are 164 M and 873 M times, respectively, slower than the LJ timing. Thus they are five or six orders of magnitude more costly than the most expensive many-body potentials in Table I. Moreover, they indicate that unlike the empirical many-body potentials, DFT calculations do not yet scale linearly with the number of atoms (or electrons). Thus for DFT simulations of 32 K- or 1 M-atom systems, as benchmarked for the atomistic case, these ratios would be many orders of magnitude larger.

Science examples

In this section, we give brief descriptions and images from four recent large-scale simulations using the MEAM, AIREBO, and ReaxFF potentials discussed in the previous section. These were all performed on large parallel machines, using hundreds to thousands of processors and with various parallel molecular dynamics (MD) codes.

Figure 3 shows the tree-like structure of displaced atoms in a bulk plutonium (Pu) sample resulting from the recoil energy imparted to a single atom by an α-decay event as modeled in Reference 31. Simulations with up to 16 M atoms (a 75 nm cube) were run for 2 ns to track the resulting damage and energy deposition. The MEAM potential[9] was used since it accurately models a variety of Pu phases by including angle-dependent density contributions from electrons occupying *p*, *d*, and *f* orbitals. These simulations were done with the pDynamo code developed by the authors,[31] a parallel version of the original EAM DYNAMO code. One interesting result from the modeling was the temperature dependence of the damage persistence. At 600 K, damage slowly heals, and bulk crystal structure is recovered; at 180 K, an amorphous glass-like structure is created.

Figure 4 depicts the initial configuration of a model of fiber bundles composed of carbon nanotubes (CNTs) of varying individual length, arrayed end-to-end with cross-linking atoms and bonds added randomly between laterally adjacent CNTs, as described in Reference 32. The largest systems studied were 800 nm length fibers, with 1.2 M total atoms. Strain was applied incrementally along the axis of the fiber (with relaxation time between the strain increments) over time scales up to 6 ns to measure the stress in the fiber and observe its eventual rupture, as at the bottom of Figure 4. The AIREBO potential[12] was employed, as it has been widely used for CNT modeling and allows C–C bonds to spontaneously form and break. These simulations were run with the LAMMPS code discussed in the previous section.[19] Tensile strengths (at breakage) increased with fiber length and cross-linking density, with a value of 60 GPa observed for 800 nm fibers with cross-links involving 0.75% of the CNT atoms.[§] This compares with a tensile strength of 110 GPa for single (5,5) CNTs used to construct the fiber.

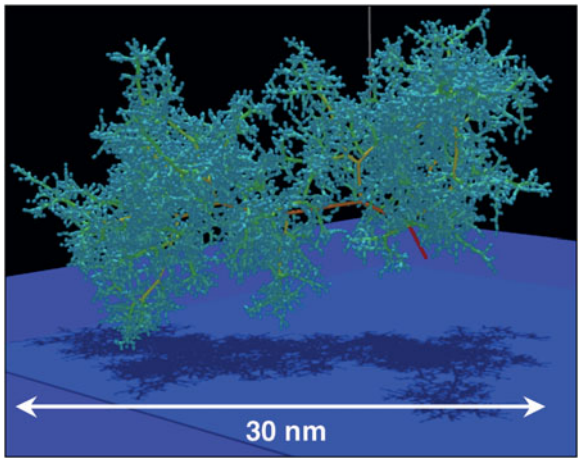

Figure 3. Tree structure of an 85 keV collision cascade in δ-Pu at 600 K, simulated with a modified embedded-atom method potential. The colors represent the kinetic energy of the atom; red = high, yellow = medium, green = low. Reprinted with permission from Reference 31. ©2007, Springer Science + Business Media.

Figure 5 illustrates simulations used to elucidate atomistic mechanisms responsible for sulfur segregation–induced embrittlement of polycrystalline nickel, presented in Reference 33. The ReaxFF potential[14] was used to capture the stress-induced reactions occurring between Ni and S near the grain boundaries (GBs). Models with 48 M atoms (2048 grains) were constructed for both pure Ni and Ni with 20% S in 1-nm-thick layers around the GBs. The models were large in the *xy* dimensions (470 nm) and thin and periodic in *z* (5 nm) to model a columnar grain structure. Lateral strain was applied in the vertical direction of Figure 5 to a notched sample, and fracture ensued over the course of 0.25 ns simulations performed with a parallel code developed by the authors.[33]

The pure Ni sample (Figure 5, upper left) fractured in a ductile manner with crack-tip blunting and void formation.

[§] For comparison, high-strength steel has a tensile strength of ~2 GPa; Kevlar is ~3.5 GPa.

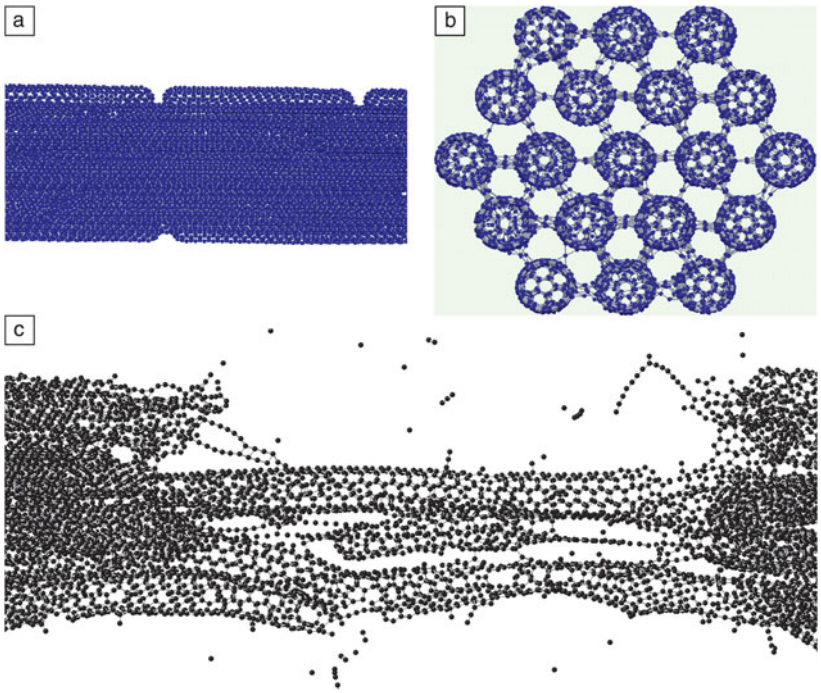

Figure 4. Fracture of a bundle of carbon nanotubes (800 nm in length) undergoing tensile strain, simulated with the adaptive intermolecular reactive empirical bond-order potential. (a) A side view of a portion of the unstrained fiber; (b) an end view showing cross-links between fibers; and (c) after fracture occurs, with strain applied in the lateral direction. Reprinted with permission from Reference 32. ©2011, American Institute of Physics.

In contrast, the S-doped sample (upper right) fractured in a brittle manner, exhibiting only intergranular cleavage. Because atomistic simulations give the time histories of all atoms, further analysis was possible, as illustrated at the bottom of the figure. The common neighborhood parameter[34] illuminates atomic-scale defects such as dislocations as they form and move. Localized stress and energy calculations can also be performed. The authors' analysis indicated a two-fold mechanism for S-embrittlement: a reduction in GB tensile strength, as well as a dramatic reduction in GB shear strength due to amorphization of the Ni-S phases present at the boundaries.

Finally, **Figure 6** shows results from non-equilibrium MD simulations of the shock compression of a polymer foam constructed from several thousand 50-mer chains of poly(4-methyl-1-pentene) (PMP), as described in Reference 35. An fcc lattice of 16 nm diameter voids was introduced by growing spherical inclusions into dense samples to give an initial density of 0.3 g/cc, as at the top of the figure. The largest models were 20 x 20 x 80 nm^3 in size and periodic in the lateral dimensions with 1.44 M atoms. A piston strikes the sample from the left at velocities up to 30 km/s. The simulations were performed with LAMMPS[19] using the ReaxFF potential[14] to allow for dissociation of the polymer bonds. A small time step of 0.025 fsec was required due to the high temperatures induced, and the shock front was tracked over a time scale of tens of picoseconds.

The bottom of Figure 6 shows the shock front, which ruptures polymer bonds and induces jetting of polymer fragments into the voids. This is in contrast to shock propagation in dense samples, which gives rise to little dissociation. The model quantitatively captures the pressure/density relationship of the material in the strong shock regime, in good agreement with experiment. The atomistic simulations also allow direct calculation of local temperature fluctuations and hot spot formation around the voids, effects that are difficult to measure experimentally.

Future issues

One software issue with using complex many-body potentials in atomistic modeling codes is that "development" is a continual process. The kernel of a Lennard-Jones potential is 10 lines of code, whereas it is thousands of lines for a potential such as ReaxFF. As bugs are found, or features added, or upgrades made by developers implementing a potential in different codes, it can be hard for users to know which version they have or which version was used in a published result. This is particularly true for many-body potentials, where their application to new materials of interest (e.g., alloys, see the Pastewka et al. article in this issue) translates to large collections of material-specific input and fitting parameters that must be carefully replicated to reproduce simulation results. The Knowledgebase of Interatomic Models (KIM) project[36] hopes to address these kinds of issues by providing a repository where multiple versions of many-body (and other) potentials can be time-stamped and archived, and then used by various atomistic modeling codes via a standardized interface.

On the hardware side, two trends in high-performance computing are changing the computer architectures that materials modeling codes (of all kinds, not just molecular dynamics) will commonly be running on in the future, at least at the high end.

The first is the advent of graphics processing units (GPUs) and other highly threaded many-core processors from chip makers such as NVIDIA and Intel that are increasingly attractive for scientific computing. The second is the push for exascale computing by the US Department of Energy (and other government agencies in the United States and worldwide). In this context, "exascale" means large machines, 1000x more powerful than today's state-of-the-art petascale machines (peta = 10^{15} floating point operations per second). Aiming for maximum floating-point performance (flops) at low cost on a few-year timeframe is driving the design and commissioning of "hybrid" supercomputers, whose compute nodes contain both many-core CPUs and GPUs.

Extracting high performance from these machines will require a different style of programming, both for algorithm

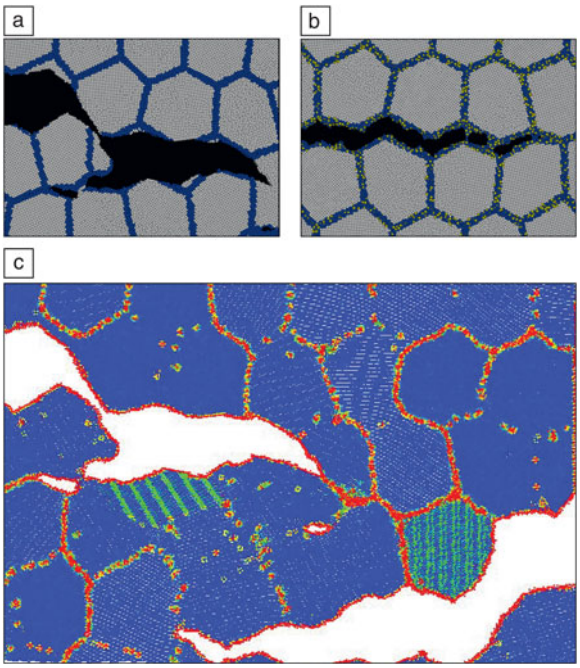

Figure 5. Ductile fracture of a polycrystalline sample (10 nm grains) of (a) pure Ni versus (b) brittle fracture of Ni with 20% S-doped (yellow atoms) grain boundary layers. (c) The bottom view of the pure Ni simulation is colored via the common neighborhood parameter[34] to highlight defects (non-blue) appearing at different scales. Reprinted with permission from Reference 33. ©2010, American Physical Society.

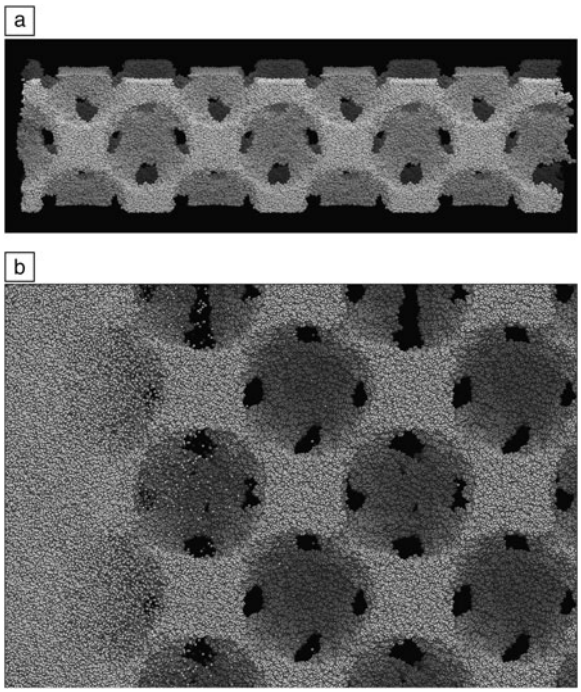

Figure 6. Shock compression response of a low-density polymer foam,[35] simulated using the reactive force field potential.[14] (a) The initial 80-nm length foam sample and void structure. (b) A magnified view of the shock wave moving from left to right through the sample. The dark patches are locations where the voids connect to adjacent voids on the back side of the sample. Small molecular fragments are ejected into the void space ahead of the main shock front.

design and low-level coding. Parallelism will need to be exploited at several levels (vector operations, multi-threading, message-passing), and memory access will need to be controlled and optimized across a hierarchy of latency times and bandwidths. Computational tasks will need to be partitioned and balanced across a mixture of cores and GPUs that perform at different rates. Considerable work has already been done on these fronts to optimize molecular dynamics simulations with pairwise potentials.[37–40] But these are harder challenges for many-body potentials due to their complexity. The computational intensity of many-body potentials may translate into large speedups when they are optimized for GPUs; this is an area of active research.

We note one ancillary benefit of the trend whereby many-body potentials are becoming more expensive. On large parallel machines, a higher computational cost (per atom, relative to communication), typically means higher parallel efficiencies can be maintained with fewer atoms per core. Thus, for a simulation of a given size, the more expensive the potential, the more processors can be used efficiently. One counterbalance is that potentials with a long-range component (e.g., Coulombics) often run less efficiently with fewer atoms per processor. It is still an outstanding challenge to efficiently solve for long-range Coulombics on large numbers of processors using either FFT-based or multipole or multigrid solvers.

If the materials science community is successful in fully exploiting the capabilities of next-generation hardware for materials modeling, one outcome may be foreseen from recent successes in biomolecular modeling. New serial and parallel algorithms aimed at efficient simulation of "small" systems (e.g., tens of thousands of atoms for small solvated proteins) and the design of specialized hardware tuned for this problem, such as the Anton machine of D.E. Shaw Research, have recently enabled simulations of protein folding at the millisecond time scale (400 billion 2.5-fsec time steps!).[41] This is allowing direct comparison with experiment, which in turn is enabling quantitative testing and improvement in the accuracy of force fields such as CHARMM[5] and AMBER,[6] which have been used for decades in biomolecular simulations. Similar opportunities would be welcomed by developers and users of many-body potentials for materials systems.

Looking further ahead, the continued advance of computing power, coupled with innovative development of more accurate and robust many-body potentials, portends an exciting next 30 years for materials modeling. Perhaps our community can achieve the Pixar-like goal of modeling any material with quantitative atomic level accuracy via empirical potentials, at length and time scales limited only by computing resources, and all with a minimum effort by the simulator.

Acknowledgments

We thank the following collaborators for their implementation of many-body potentials in LAMMPS that we discussed: Tzu-Ray Shan (COMB, U Florida/SNL), Metin Aktulga (ReaxFF, LBNL), Greg Wagner (MEAM, SNL), Don Ward (BOP, SNL), and Ase Henry (AIREBO and REBO, Georgia Tech). We also thank Alison Kubota (SNL), Charles Cornwell (US Army ERDC), Priya Vashishta (USC), and Matt Lane (SNL) for providing figures to acompany discussion of their work.

References

1. Pixar Animation Studios; www.pixar.com.
2. M. Pickavance, online posting, www.denofgeek.com/movies/417298/the_cgi_achievements_of_pixar.html (accessed March 2012).
3. C. Good, online posting; www.quora.com/Toy-Story-movie-series/How-much-faster-would-it-be-to-render-Toy-Story-in-2011-compared-to-how-long-it-took-in-1995 (accessed March 2012).
4. J.E. Jones, *Proc. R. Soc. London, Ser. A* **106**, 463 (1924).
5. A.D. MacKerell Jr., D. Bashford, M. Bellott, R.L. Dunbrack Jr., J.D. Evanseck, M.J. Field, S. Fischer, J. Gao, H. Guo, S. Ha, D. Joseph-McCarthy, L. Kuchnir, K. Kuczera, F.T.K. Lau, C. Mattos, S. Michnick, T. Ngo, D.T. Nguyen, B. Prodhom, W.E. Reiher III, B. Roux, M. Schlenkrich, J.C. Smith, R. Stote, J. Straub, M. Watanabe, J. Wirkiewicz-Kuczera, D. Yin, M. Karplus, *J. Phys. Chem. B* **102**, 3586 (1998).
6. T.E. Cheatham III, M.A. Young, *Biopolymers* **56**, 232 (2001).
7. M.S. Daw, M.I. Baskes, *Phys. Rev. Lett.* **50**, 1285 (1983).
8. M.S. Daw, M.I. Baskes, *Phys. Rev. B* **29**, 6443 (1984).
9. M.I. Baskes, *Phys. Rev. Lett.* **59**, 2666 (1987).
10. J. Tersoff, *Phys. Rev. B* **37**, 6991 (1988).
11. D.W. Brenner, *Phys. Rev. B* **42**, 9458 (1990).
12. S.J. Stuart, A.B. Tutein, J.A. Harrison. *J. Chem. Phys.* **112**, 6472 (2000).
13. D.G. Pettifor, I.I. Oleinik, *Phys. Rev. B* **59**, 8487 (1999).
14. A.C.T. van Duin, S. Dasgupta, F. Lorant, W.A. Goddard III, *J. Phys. Chem. A* **105**, 9396 (2001).
15. J. Yu, S.B. Sinnott, S.R. Phillpot, *Phys. Rev. B* **75**, 085311 (2007).
16. S.W. Rick, S.J. Stuart, B.J. Berne, *J. Chem. Phys.* **101**, 16141 (1994).
17. D. Wolf, P. Keblinski, S.R. Phillpot, J. Eggebrecht, *J. Chem. Phys.* **110**, 8254 (1999).
18. P. Ewald, *Ann. Phys.* **369**, 253–287 (1921).
19. LAMMPS molecular dynamics package, http://lammps.sandia.gov; Potential benchmarks, http://lammps.sandia.gov/bench.html#potentials.
20. S. Plimpton, *J. Comp. Phys.* **117**, 1 (1995).
21. D.W. Brenner, O.A. Shenderova, J.A. Harrison, S.J. Stuart, B. Ni, S.B. Sinnott, *J. Phys. Condens. Matter* **14**, 783 (2002).
22. T.-R. Shan, B.D. Devine, T.W. Kemper, S.B. Sinnott, S.R. Phillpot, *Phys. Rev. B* **81**, 125328 (2010).
23. A.P. Thompson, S.J. Plimpton, W. Mattson, *J. Chem. Phys.* **131**, 154107 (2009).
24. R.W. Hockney, J.W. Eastwood, *Computer Simulation Using Particles* (IOP, Bristol, 1988).
25. E.L. Pollock, J. Glosli, *Comput. Phys. Commun.* **95**, 93 (1996).
26. T. Darden, D. York, L. Pedersen, *J. Chem. Phys.* **98**, 10089 (1993).
27. A.P. Bártok, M.C. Payne, R. Kondor, G. Csányi, *Phys. Rev. Lett.* **104**, 136403 (2010).
28. T.R. Mattsson, M.P. Desjarlais, *Phys. Rev. Lett.* **97** (1) (2006).
29. S. Root, R.J. Magyar, J.H. Carpenter, D.L. Hanson, T.R. Mattsson, *Phys. Rev. Lett.* **105** (8) (2010).
30. G. Kresse, J. Hafner, *Phys. Rev. B* **49** (20), 14251 (1994).
31. A. Kubota, W.G. Wolfer, S.M. Valone, M.I. Baskes, *J. Comput.-Aided Mater. Des.* **14**, 367 (2007).
32. C.F. Cornwell, C.R. Welch, *J. Chem. Phys.* **134**, 204708 (2011).
33. H.P. Chen, R.K. Kalia, E. Kaxiras, G. Lu, A. Nakano, K. Nomura, A.C.T. van Duin, P. Vashishta, Z. Yuan, *Phys. Rev. Lett.* **104**, 155502 (2010).
34. H. Tsuzuki, P.S. Branicio, J.P. Rino. *Comput. Phys. Commun.* **177**, 518 (2007).
35. J.M.D. Lane, G.S. Grest, A.P. Thompson, K.R. Cochrane, M.P. Desjarlais, T.R. Mattsson, in *AIP Conference Proceedings, Shock Compression of Condensed Matter 2011*, M. Elert, W.T. Buttler, J.P. Borg, J.L. Jordan, T.J. Vogler, Eds., vol. 1426, p. 1435 (2012).
36. Knowledgebase of Interatomic Models (KIM); www.openkim.org.
37. J.A. Anderson, C.D. Lorenz, A. Travesset, *J. Comput. Phys.* **227**, 5342 (2008).
38. W.M. Brown, A. Kohlmeyer, S.J. Plimpton, A.N. Tharringon, *Comput. Phys. Commun.* **183**, 449 (2012).
39. W.M. Brown, P. Wang, S.J. Plimpton, A.N. Tharrington, *Comput. Phys. Commun.* **182** (4), 898 (2011).
40. J.E. Stone, J.C. Phillips, P.L. Freddolino, D.J. Hardy, L.G. Trabuco, K. Schulten, *J. Comput. Chem.* **28** (16), 2618 (2007).
41. D.E. Shaw, P. Maragakis, K. Lindorff-Larsen, S. Piana, R.O. Dror, M.P. Eastwood, J.A. Bank, J.M. Jumper, J.K. Salmon, Y.B. Shan, W. Wriggers, *Science* **330**, 341 (2010).
42. H.J.C. Berendsen, J.R. Grigera, T.P. Straatsma, *J. Phys. Chem.* **91**, 6269 (1987). □

XXI INTERNATIONAL MATERIALS RESEARCH CONGRESS (IMRC) 2012
August 13–17, 2012 • Cancun, Mexico
A joint meeting of the **Sociedad Mexicana de Materiales** and the **Materials Research Society**

SYMPOSIA

Nano Science and Technology
1A Low-Dimensional Bismuth-Based Materials*
1B Nanostructured Carbon Materials for MEMS/NEMS and Nanoelectronics*
1C Nanostructured Materials and Nanotechnology
Metals Characterization
2A The Role of Surfaces and Interfaces in Materials Processes*
2B Novel Characterization Methods for Biological Systems*
2C Quantitative Measurements with Atomic Force Microscopy in Fluids*
2D Structural and Chemical Characterization of Metals, Alloys, and Compounds
Materials for Energy Production
3A Materials for Polymer Electrolyte Membrane Fuel Cells*
3B Photocatalytic and Photoelectrochemical Nanomaterials for Sustainable Energy*
3C Photovoltaics, Solar Energy Materials, and Technologies
3D New Catalytic Materials
3E Renewable Energy and Sustainable Development
Biomaterials
4A Nanotechnology-Enhanced Biomaterials and Biomedical Devices*
4B Biomaterials for Medical Applications
Polymers
5A Soft Responsive Materials*
5B New Trends in Polymer Chemistry and Characterization
Electronics and Photonics
6A Organic Materials for Electronics and Photonics*
6B Low-Dimensional Semiconductor Structures*
6C Advances in Semiconducting Materials
6D Materials and Devices for Large-Area Electronics*
Fundamental Materials Science
7A Advances in Computational Materials Science
7B Concrete with Smart Additives and Supplementary Cementitious Materials*
7C NACE: Corrosion and Metallurgy
7D Advanced Structural Materials
7E Interfaces, Structure, and Domain Engineering in Ferroic Systems*
7F Solid-State Chemistry of Functional Inorganic Materials*
General
8A Strategies for Academy-Industry Relationship

**Sponsored jointly by MRS and SMM*

Register today at www.mrs.org/IMRC2012